Permanent indentation characterization for low-velocity impact modelling using three-point bending test

Natthawat Hongkarnjanakul, Samuel Rivallant, Christophe Bouvet, Arturo Miranda

Permanent indentation characterization for low-velocity impact modelling using three-point bending test

Natthawat Hongkarnjanakul, Samuel Rivallant, Christophe Bouvet and Arturo Miranda

Abstract

This paper deals with the origin of permanent indentation in composite laminates subjected to low-velocity impact. The three-point bending test is used to exhibit a non-closure of matrix crack which is assumed as a cause of permanent indentation. According to the observation at microscopic level, this non-closure of crack is produced by the blocking of debris inside matrix cracking and the formation of cusps where mixed-mode delamination occurs. A simple physically-based law of permanent indentation, "pseudo-plasticity", is proposed. This law is qualitatively tested by three-point bending finite element model and is lastly applied in low-velocity impact finite element model in order to predict the permanent indentation. A comparison between low-velocity impact experiments and simulations is presented.

Keywords

Permanent indentation, dent depth, impact behaviour, damage mechanics, damage tolerance, three-point bending test

Introduction

In recent years, the use of composite structures has increased in aeronautical and aerospace applications, thanks to their high specific strength and stiffness with weight reduction. However, the brittleness of the composites is reflected in their poor ability to resist impact damage that might be encountered in accidental situations such as tool drops during manufacturing or maintenance, etc. This can cause a severe reduction of strength of the structure both in tension and compression. However, the difficulty to detect internal damage is a more sensitive aspect due to unobvious visible sign on the surface. This has led to a fundamental design concept for damage tolerance of aeronautic structures. To achieve damage tolerance requirement, when the damage does occur but is invisible, composite parts must have sufficient residual strength to resist failure at design ultimate load. As a result, "barely visible impact damage" (BVID) is defined as level at which the damage is detectable.[1] In practice, the BVID is commonly inspected by measuring "dent depth" or "permanent indentation," which is specified as a difference between the lowest point in the dent and the surface.[2] Understanding of permanent indentation mechanism is therefore essential to allow for designing the composite structures with respect to damage tolerance. In the last decades, a number of researchers have studied damage due to low-velocity impact[3–7]; however, the phenomenon of permanent indentation is still not very well understood.[4,5,8–12] Therefore, the argument of indentation mechanism is still open.

In literature, some analytical predictions and indentation models have been proposed. Caprino et al.[9,10] experimentally studied low-velocity impact on composite laminates and found that if the ratio of impact energy to the penetration energy, which is unaffected by the loading speed, is known, the permanent indentation can be evaluated, regardless of laminate type and thickness. The prediction of permanent indentation is accomplished by an exponential equation based on the best-fit method from available experimental data. The question arises whether this approach is valid when laminate configurations/materials are changed. Hence,

Université de Toulouse: ISAE, INSA, UPS, Emac; ICA (Institut Clément Ader), Toulouse, France

Corresponding author:
Natthawat Hongkarnjanakul, ISAE (Institut Supérieur de l'Aéronautique et de l'Espace); 10 Avenue Edouard Belin, BP 54032, 31055 Toulouse Cedex 4, France.
Email: natthawat.h@gmail.com

other methods should also be considered such as finite element (FE) analysis. For example, a simulation of low-velocity impact damage and permanent indentation based on continuum damage mechanics, as reported in Ref [5–7]. The permanent indentation mechanism is included in the non-linear shear behaviour which is decomposed into (1) elastic undamaged, (2) elastic damaged and (3) inelastic damaged components. Irreversibility of the last term is attributed to unclosed cracks and causes the formation of permanent indentation. These models consist of fracture mechanics approach with damage evolution. Thus, shear fracture toughness under intralaminar matrix failure needs to be measured. Nevertheless, this value is difficult to evaluate,[13] especially out-of-plane shear behaviour which is a fundamental direction for the formation of permanent indentation. As a result, Donadon et al.[5] simply assumed out-of-plane shear behaviour to be identical to in-plane shear behaviour for their fabric laminates because of the lack of experimental results for out-of-plane shear behaviour, thus some limitations for this assumption might be of concern.

The value of permanent indentation significantly increases when fibre failure is detected.[11,12] On the other hand, at a small value of permanent indentation, a small amount of fibre failure is observed. The permanent indentation is probably driven by plasticity of resin ductility/non-linear shear behaviour and matrix cracking. To model all these complex mechanisms of permanent indentation, i.e. fibre failure, matrix cracking/plasticity, He et al.[12] have proposed a model of permanent indentation associated with anisotropic elasto-plasticity theory in continuum mechanics, but five internal coefficients for the shear model need the trial and error optimization. Excellent predictions of permanent indentation value in function of impact energy for two tested material systems are presented. Also, the importance of fibre failure affecting permanent indentation was also shown in Bouvet et al.'s[4] simulation on the evolution of impact energy, even if their permanent indentation law is associated with matrix cracking rather than fibre failure. In fact, this law is based on an experimental investigation from Abi Abdallah et al.[8] who claimed that the permanent indentation is formed because the debris get stuck inside matrix cracking void (Figure 1). These debris play an important role to block the closure of matrix cracks returning to initial position. The accumulation of these opening of matrix cracks in each ply can contribute to the formation of permanent indentation. Moreover, during an impact event, fibre failure can locally degrade the plies' rigidity and cause a great opening of these matrix cracks and delamination. This can indirectly affect the permanent indentation to be more significant. Thanks to this assumption,

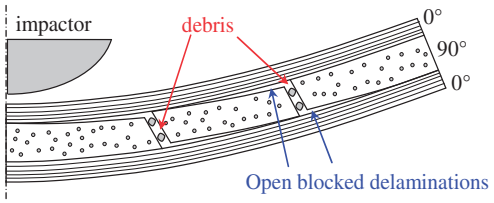

Figure 1. The principle of creation of permanent indentation.[3]

Table 1. Specimen configurations.

Name	Layups	Thickness, h (mm)
I1	$[0, 90_6, 0]$	2.0
I2-A	$[0_2, 90_2, 0_2]$	1.5
I2-B	$[0_2, 90_2, 0_2]$	1.5
I2-C	$[0_2, 90_2, 0_2]$	1.5

Bouvet et al.[3,4] are able to present accurate simulation results for their test cases, for example the indentation value, and deformed shape of the plate. However, two necessary parameters in their simulation i.e. debris size and debris stiffness are assumed and not yet identified.

Due to lack of explanation on physical basis of permanent indentation in literature, the aim of this current paper is to clarify this point in order to improve the permanent indentation response on low-velocity impact simulation[3,4] and to propose a way to identify parameters governing permanent indentation. Thus, a three-point bending test is chosen for this study, which enables the creation of matrix cracks and follows their evolution: opening, closure and eventual blocking of closure. Mechanism of crack opening/closure particularly in out-of-plane direction is highlighted, which can lead to new interpretation and understanding of the formation of permanent indentation. A simple law of permanent indentation is presented, and a single required parameter is proposed, based upon experiment-model identification. The final step is to verify this indentation law on impact model and validate on test cases.

Experimental

Material and test setup

Three-point bending tests are conducted under hydraulic machine at a displacement rate of 0.3 mm/min. Specimens with a dimension of $50 \times 10\,\text{mm}^2$ (length × width) are made of T700/M21 (carbon-epoxy). Two stacking sequence configurations of specimens are detailed in Table 1, which particularly enable the observation of matrix cracking in the internal plies

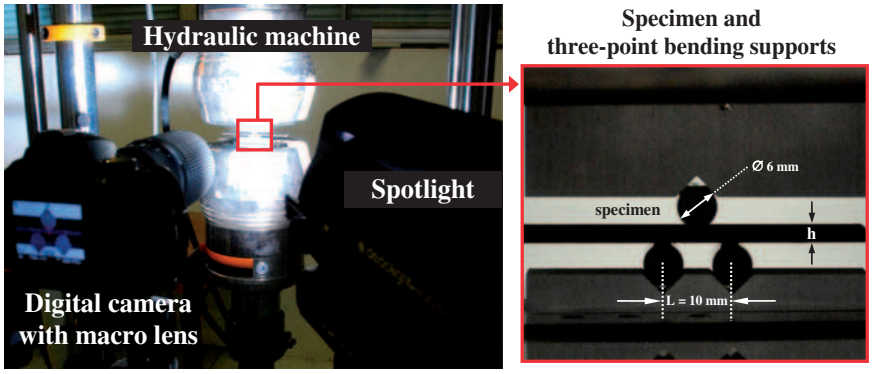

Figure 2. Three-point bending test setup.

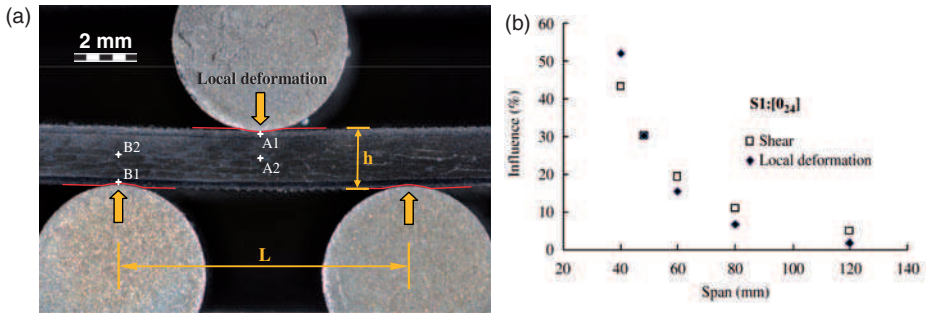

Figure 3. Demonstration of local deformation effect on three-point bending test (a) present test on specimen 11 and (b) relative influence of local deformation and shear effects with respect to bending.[15]

oriented at 90°. To predominantly generate the matrix cracking at the 90° plies (generally coupling with delamination) due to shear with less possibility to have tensile or compressive fibre failure of 0° external plies, the span (distance between the two lower supports) to thickness ratio (L/h) should be reduced.[14] Thus, 10 mm of span and three cylinder supports of 6 mm of diameter are chosen for this study (Figure 2).

During the three-point bending test, a digital camera with macro lens meanwhile captures in the section of specimen being affected with an automatic interval timer function. These images are then post-analysed using image correlation technique in order to observe the translation of deformed specimens and their cracks. Since the physical basis of the mechanism of permanent indentation is initially assumed due to the debris which may block the crack closure,[8] crack void and debris should be observed in optical microscope. Therefore, each specimen must be polished before test to ensure that the debris observed does not come from small particles during polish process (generally done after test). Moreover, areas of interest are photographed by scanning electron microscope (SEM) in order to observe more precisely the debris.

Three-point bending test and local deformation

As a result of reducing the span in three-point bending test to favour the crack in 90° plies, consequent influences must be taken into account i.e. relatively high shear effect, and high local contact pressure of the specimen against cylinder supports, known as "local deformation" (Figure 3(a)). In particular, if the specimen has small span and large thickness, the local deformation effect will be very significant comparing to shear and bending effects[15] (Figure 3(b)). In order to later analyze the three-point bending from FE model (cf. section §3) which does not take into account the local deformation, and highlights shear and bending behaviour, the effect of local deformation should be minimized as much as possible.

The displacement obtained from the machine can be defined as the global displacement, δ^{global}. This quantity can be subdivided into two components namely the bending displacement, $\delta^{bending}$, where shear effect is also included, and the local deformation, δ^{local}.

$$\delta^{global} = \delta^{bending} + \delta^{local}. \quad (1)$$

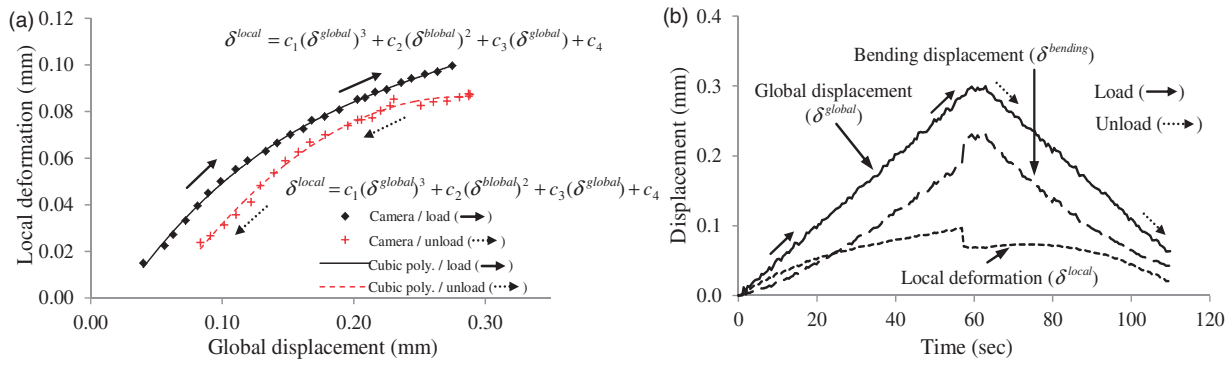

Figure 4. Displacement output data of specimen I1 (a) local deformation in function of global displacement from image correlation technique and cubic polynomial estimation and (b) different types of displacement during three-point bending test.

The bending displacement cannot directly be measured but it can be evaluated if the global displacement and the local deformation are known (equation 1). Thanks to the image correlation technique in 2D, the global displacement can be determined by monitoring the movement on the cylinder supports. Also, the local deformation can be simply evaluated by measuring the different displacement between cylinder contact noses and neutral axis of the specimen, at points A1, A2, B1 and B2, as shown in Figure 3(a).

$$\delta^{local} = |\Delta_{A1} - \Delta_{A2}| + |\Delta_{B1} - \Delta_{B2}| \qquad (2)$$

where Δ_{A1}, Δ_{A2}, Δ_{B1} and Δ_{B2} are the vertical displacements at point A1, A2, B1 and B2, respectively. The software then interprets the difference from the series of images and gives the results of displacements in pixel units; these displacements can consequently be converted to mm. Nevertheless, the acquisition frequencies for global displacement – obtained from hydraulic machine – and for image correlation are different. Thus, the displacement measures from image correlation are fitted by a cubic polynomial interpolation (Figure 4(a)). Lastly, the bending displacement is obtained, as shown in Figure 4(b). Hereafter in this paper, unless otherwise specified, the term ''displacement'' means the bending displacement rather than the global displacement.

Opening and closure of matrix crack

The evolution of crack opening/closure is studied according to previous observation of formation of permanent indentation proposed by Abi Abdallah et al.[8] Similarly to what occurs in an impact event including a loading and a rebound, three-point bending test is carried out with only one cycle of loading and unloading. Many tests were performed, but unfortunately, it is quite complex to control the formation of a unique crack in the specimen, to avoid uncertain crack location, or even to avoid fibre rupture under the indentor. Only specimens with a single crack and no fibre rupture were analysed, so that only the influence of matrix cracks could be studied. Finally, only four interesting specimens are chosen. The results from three-point bending test of specimen I1 are presented in Figure 5. The specimen is loaded until the appearance of a 45° matrix cracking (normally coupling with delamination), which can be noticed due to the dramatic load drop at state 2–3. When the matrix crack occurs, the specimen's internal rigidity suddenly decreased but the global displacement remains the same. As a consequence, the local deformation is released and leads the bending displacement shift at state 2–3 (see also the displacement relation in Figure 4(b)). The out-of-plane crack width δ_z is also measured by using image correlation technique (same technique as determining the local deformation). Unloading is then applied and the crack width gets smaller (state 3-4-5). At the end of the test (point 5), one can notice that there is a residual crack opening when the force is null. This phenomenon is assumed to be the basis of the formation of permanent indentation.

If this unclosed crack leads to the formation of permanent indentation, it is questionable as to what mechanisms influence the Residual crack opening width. Three additional tests on configuration I2 are consequently performed but different load cases are introduced. The load is continuously applied after the onset of crack initiation and before the presence of fibre failure to three different levels of added displacements, i.e. 0.02 mm, 0.08 mm and 0.15 mm for specimens I2-A, I2-B and I2-C, respectively (Figure 6(a)). The results exhibit some scatters in the onset of crack formation data for these tests, but different crack widths are investigated according to the different added displacement (Figure 6(b)). There is no fixed value of the residual crack opening, but it probably depends on the maximum crack opening.

Evolution of crack opening/closure both in transverse direction δ_t, and in out-of-plane direction δ_z,

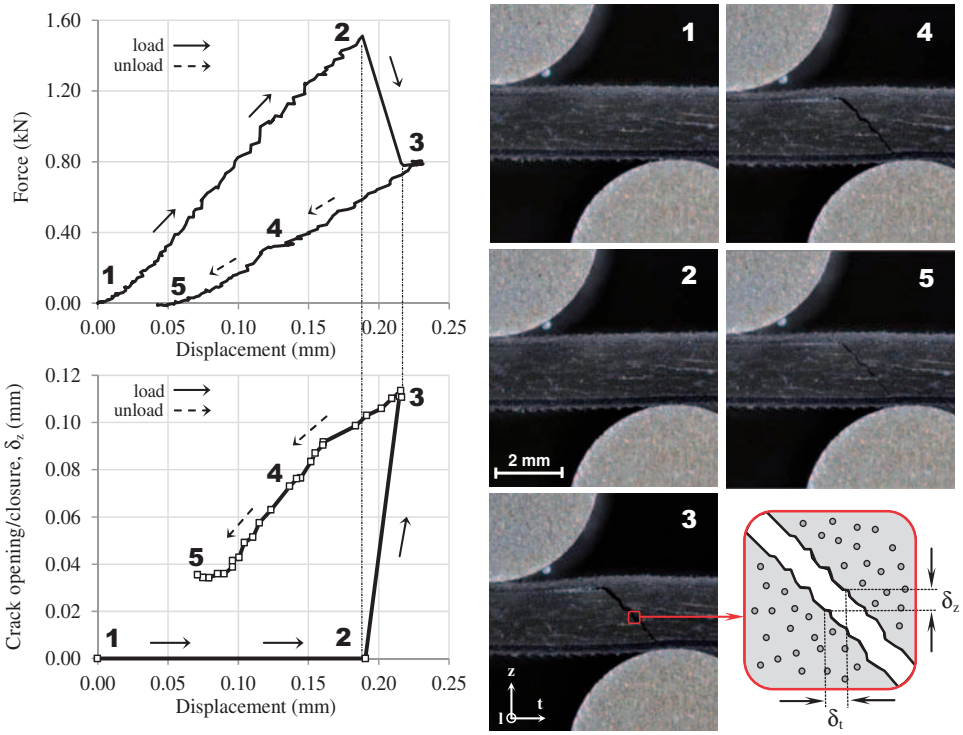

Figure 5. Observation of the evolution of crack opening/closure on the right part of specimen I1.

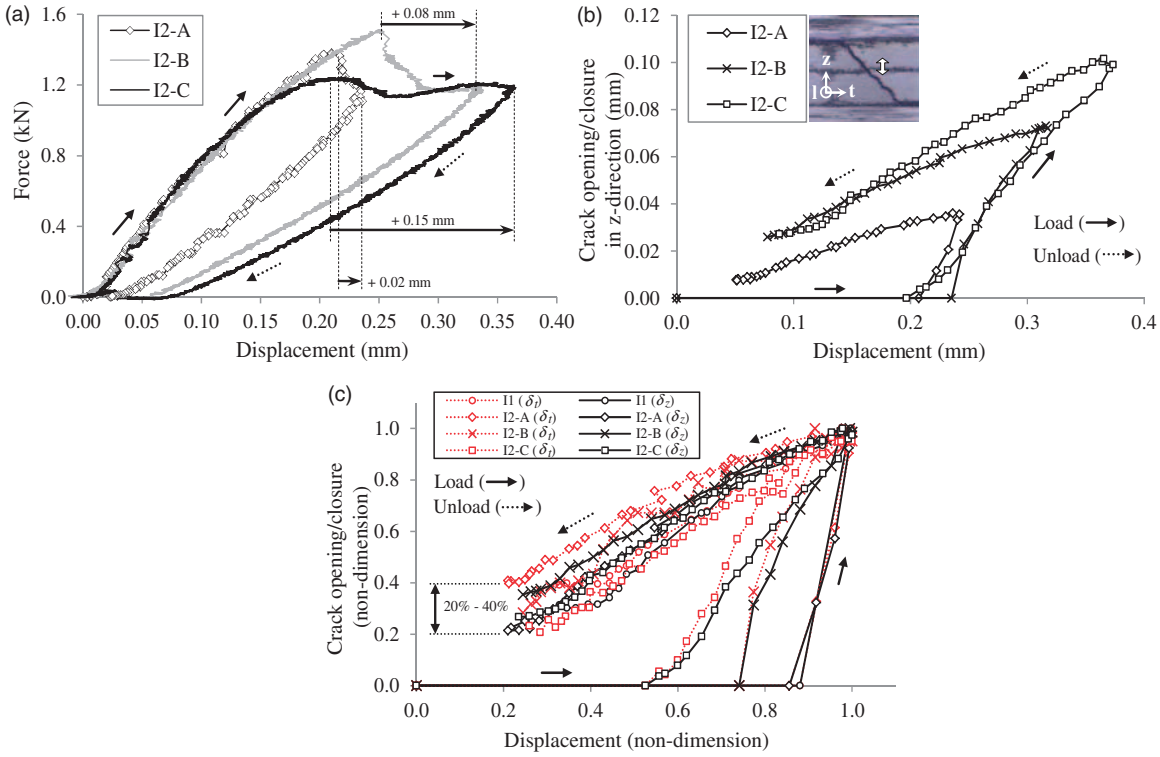

Figure 6. (a) Force-displacement for tests of specimens I2-A, B and C; (b) crack opening/closure for tests of specimens I2-A, B and C and (c) non-dimensional crack opening/closure for tests of specimens I1, I2-A, B and C.

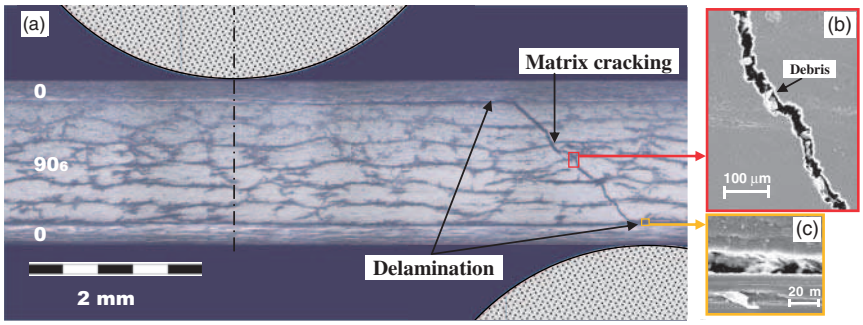

Figure 7. Post mortem observation (a) micrograph of specimen I1 after test and (b) scanning electron microscope (SEM) observation of debris inside matrix cracks; (c) SEM observation of delamination.

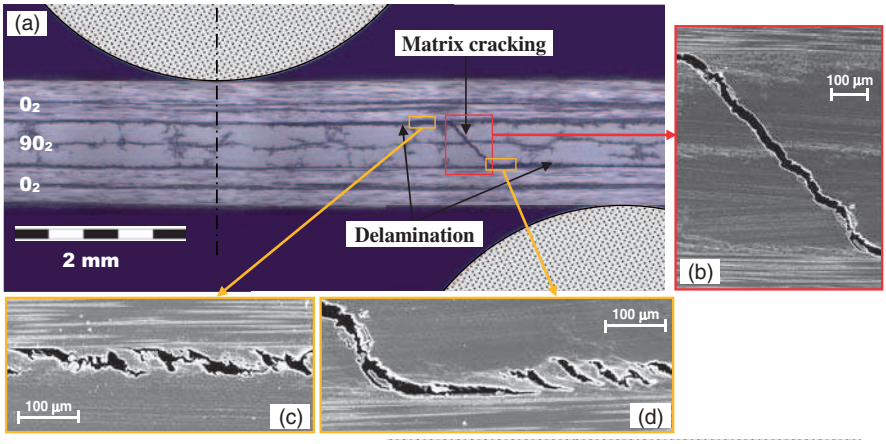

Figure 8. Post mortem observation (a) micrograph of specimen I2-B after test; (b) scanning electron microscope (SEM) observation showing a void due to matrix cracking; (c) and (d) cusps induced by delamination.

is determined at the centre of the matrix crack in the thickness direction of the specimen; the subscripts t and z denote transverse and out-of-plane directions, respectively, as demonstrated in Figure 5. The results of non-dimensional crack evolution, i.e. $\delta_t/\delta_t^{\max}$ and $\delta_z/\delta_z^{\max}$, reveal a sensible convergence for all tests. That is, using non-dimensional values of imposed displacement and crack closure, the shape of crack closure-displacement curves for all tests are similar, and regardless of how big the maximum crack opening is, the final crack closure returns to around 20%–40% of maximum crack opening (Figure 6(c)) for both crack directions (t- and z-directions) and for both specimen configurations.

In order to investigate the cause of this unclosed crack, a microscopic observation is performed. The micrographs from Figures 7(a) and 8(a) show the 45° crack appearance, and the coupling between matrix cracking and delamination for specimens I1 and I2-B, respectively. These cracks are observed at higher magnification by SEM in order to more precisely observe the crack. The debris inside the crack are clearly visible in Figure 7(b) for specimen I1 and to a lesser extent for specimen I2-B (Figure 8(b)). One must keep in mind that debris may be hidden inside the matrix cracking and are not always clearly visible from microscopic observation.

Detailed micrographs of specimen I2-B in Figure 8(c) and (d) show another mechanism leading to the non-closure of cracks. Figure 8(d) (lower interface) shows the classical formation of cusps[16] in the ply interface, due to a mixed mode delamination. In this figure, the interface of the cusps is not entirely opened, and the upper and lower plies are still linked together by packs of resin. Looking further from the delamination tip (Figure 8(c), upper interface), the cusps are completely formed and can be assimilated to debris. Both types of cusps (entirely or partially formed) will prevent the closure of delamination cracks to initial position.

According to experimental observations, we found that the main mechanisms leading to permanent indentation are both the accumulation of debris inside matrix cracks and the presence of cusps inside delamination interfaces. Moreover, measurements of the opening/

closure of cracks show that the final crack width depends on the maximum width reached during opening of the crack in the test.

Modelling of permanent indentation

Permanent indentation hypothesis

Experiments in the proceeding section demonstrate that, under unloading, different microscopic mechanisms in matrix cracks (debris) and delamination interfaces (debris, cusps) result in a global phenomenon of non-closure of the matrix cracks. From a meso-scale point of view, the final matrix crack width is found proportional to the maximum crack width reached during the test. It leads to the definition of the crack closure coefficient μ, expressed as follows:

$$\delta^0 = \mu \cdot \delta^{\max} \tag{3.1}$$

with

$$\delta^{\max}(\tau) = \max_{\tau \leq t}(\delta(\tau)) \tag{3.2}$$

where δ^0 is the final crack width, after unload, and $\delta^{\max}$ is the maximum crack width ever reached during the crack opening. t and τ are respectively the total time and the current time. The relation in equation (3.1) is a fundamental relation to drive the formation of permanent indentation, called "pseudo-plasticity" model. This law physically comprises both the blocking of debris and resin plasticity in plies. It can independently be rewritten for each crack direction: transverse and out-of-plane, without taking into account the compressive transversal direction.

$$\delta_t^0 = \mu_t \cdot \delta_t^{\max} \quad \text{if } \delta_t \geq 0 \tag{4.1}$$

$$\delta_z^0 = \begin{cases} \mu_z \cdot \delta_z^{\max} & \text{if } \delta_z \geq 0 \\ \mu_z \cdot \delta_z^{\min} & \text{if } \delta_z < 0 \end{cases} \tag{4.2}$$

where the δ_t^0, δ_z^0 are the final crack-closure width in transversal and out-of-plane directions, respectively. Furthermore, the crack closure coefficient from both directions in this study is assumed to be identical ($\mu_t = \mu_z$) due to the fact that the matrix cracks are at an angle close to 45°, which is confirmed by the results shown in Figure 6(c).

The crack evolutions are physically observed in micro-scale in terms of debris and formation of cusps, but the proposed law (equations 4.1–4.2) is responded at meso-scale in the proposed model. These law and the findings of the out-of-plane non-closure crack from previous section are comparable to the non-linear out-of-plane shear damage model proposed by Donadon et al.,[5] as shown in Figure 9. That is, the residual opening component is about 30% of maximum deformation component.

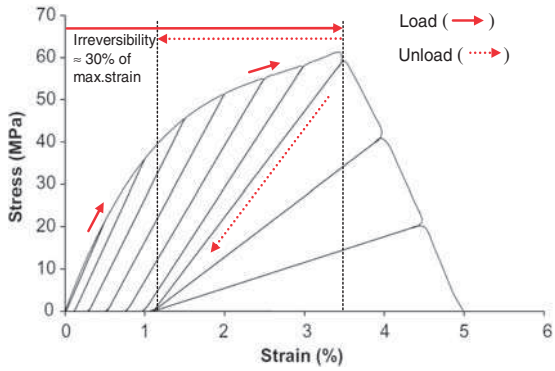

Figure 9. Non-linear in-plane and out-of-plane shear damage model from Donadon et al.[5]

Validation of permanent indentation model on three-point bending test

The objective of this section is to qualitatively test the proposed indentation law with a three-point bending FE model, and understand the interaction of crack opening/closure on the particular discrete model. Mesh types and material laws/properties are based on the impact model from Ref [3,4] in which three damage types are considered namely fibre failure, matrix cracking and delamination, as shown in Figure 10. Dynamic explicit analysis is also maintained with a reasonably slow velocity (0.1 mm/s) to eliminate dynamic problem. Since the three-point bending model is created based on the impact model, after the validation on the three-point bending model, the permanent indentation law can directly be applied to the impact model.

The experimental investigation in the previous section showed that crack non-closure is due to both matrix cracking and delamination; but at meso-scale, it can be considered as a non-closure law only applied in the matrix cracks. The permanent indentation law is integrated inside vertical interface elements where matrix cracking is assigned. To identify the damage that occurred from experiment test, only one row of interface elements is allowed to possess matrix cracking with the purpose to simulate the 45° matrix cracking (cf. Figure 13(a)–(b)). Thus, the element size was chosen according to location of the presence of 45° matrix cracking and to respect cohesive zone model for delamination. The element size for three-point bending model is about three times smaller than the reference low-velocity impact model in Ref [3,4], whereas the element's thickness is maintained the same. Figure 11 shows the mechanism of crack

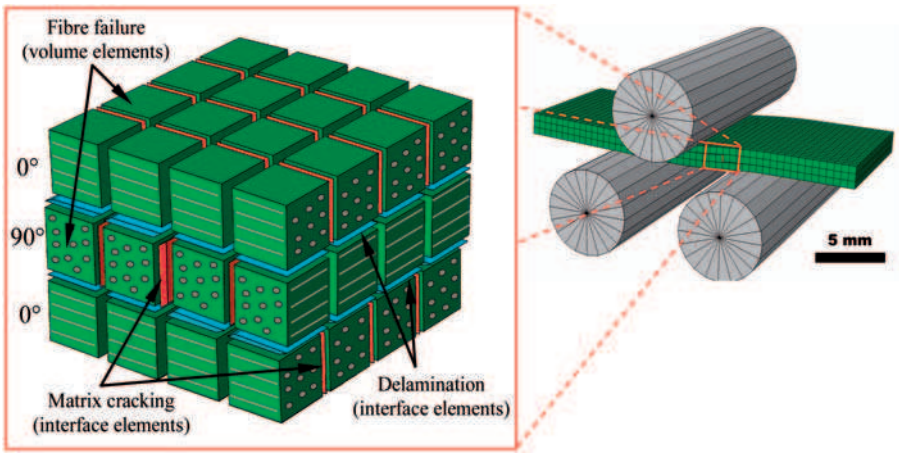

Figure 10. Three-point bending model and element types.

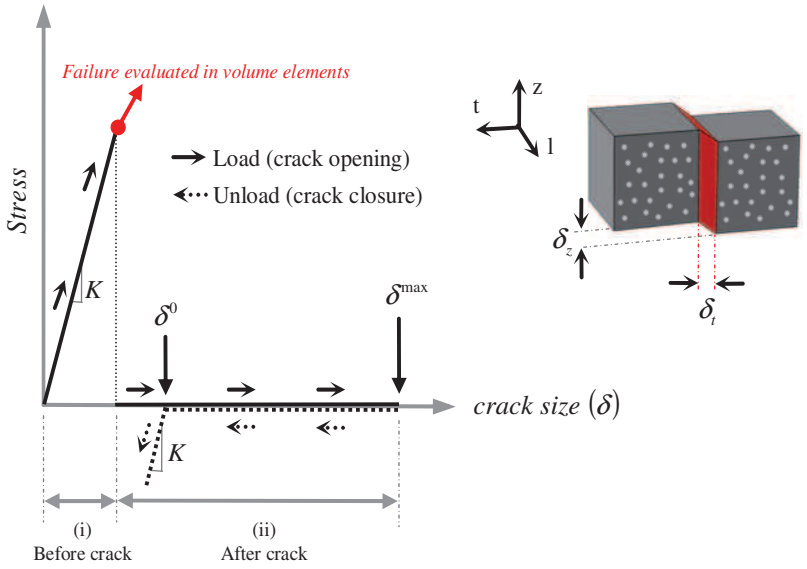

Figure 11. Permanent indentation law representing matrix cracking interface elements.

opening/closure that corresponds with the permanent indentation law in vertical interface elements.

Initiation of matrix cracking. Before reaching the onset of matrix cracking, the behaviour of vertical interface is purely elastic: the interface elements connect their neighbouring volume elements by the interface stiffness K (assumed to be very high: 500,000 MPa/mm, given in Table 2), defined in three directions:

$$\sigma_t = K \cdot \delta_t \tag{5.1}$$

$$\tau_{lt} = K \cdot \delta_l \tag{5.2}$$

$$\tau_{zt} = K \cdot \delta_z \tag{5.3}$$

The initiation of crack is governed by matrix tensile failure (equation (6)) based upon Hashin's criterion. This criterion is assigned into neighbouring volume elements, but responded in interface elements.

$$\left(\frac{\langle \sigma_t^V \rangle^+}{\sigma_t^f}\right)^2 + \frac{(\tau_{lt}^V)^2 + (\tau_{tz}^V)^2}{(\tau^f)^2} \leq 1 \tag{6}$$

where σ_t^V, τ_{lt}^V, τ_{tz}^V denote the stresses calculated in neighbour volume elements. σ_t^f the failure transverse tensile stress and τ^f is the failure in-plane shear stress. The essential mechanical characteristics of T700/M21 are given in Table 2. The purpose of this three-point bending model is to validate the crack opening/closure simulation. The failure stresses are modified to overcome the

Table 2. Mechanical characteristics of T700/M21 unidirectional ply for the three-point bending model.[17]

Ply density		1600 kg/m^3
Ply thickness		0.25 mm
E_l^{ten}	Tensile Young's modulus in fibre direction	130 GPa
E_l^{comp}	Compressive Young's modulus in fibre direction	100 GPa
E_t	Transverse Young's modulus	7.7 GPa
G_{lt}	Shear modulus	4.8 GPa
ν_{lt}	Poisson's ratio	0.33
σ_t^f	Tensile failure stress in transverse direction	60
τ^f	In-plane shear failure stress	110
K	Interface element stiffness of matrix cracking	500000 MPa/mm
μ	Crack closure coefficient	0.3

possible dispersion of rupture value in experimental tests, so that the cracks can appear at the same time for both experiment and simulation. For example, the values of σ_t^f and τ^f, for material T700/M21,[17] which equal to 60 MPa and 110 MPa, respectively (Table 2), are replaced by 39 MPa and 78 MPa for modelling case of I2-B. Moreover, another reason of the modified failure stresses is that the three-point bending model has very thick finite elements comparing to the total thickness. As a result, the estimation of shear distribution in through-thickness direction is inaccurate and complicated to predict[18]; but this problem is not evident for the reference impact model in Ref [3,4] because of a relatively thin volume element comparing to the laminate thickness. However, a modification of reducing element's thickness or adding number of element was not made in order to keep the similarity to impact model and the objective of parameter's identification.

Opening and closure of cracks. Once the matrix cracking criterion in volume elements (equation (6)) is reached (the initiation of crack), the adjacent interface elements lose their rigidity, their stresses in three directions turn to zero and the crack instantaneously opens (not taking into account the energy for propagation). Also, the delamination is automatically linked, which is performed by a conventional criterion of fracture mechanics on the horizontal interface elements. Then, after initiation of crack, the crack opening is only governed by delamination, as far as the crack width is increasing.

When the crack tends to close, during unloading, the crack closure law – presented in Figure 11 – is applied only at the interface elements for matrix cracking. As long as the crack width is larger than the final crack closure widths, δ_t^0 and δ_z^0, expressed previously, the crack freely closes with no resistant stress. But if the crack closure goes below these thresholds, the rigidity will be applied to prevent the crack closure in the z- and t- directions. The implementation of the crack closure law can be given as:

$$\sigma_t = \begin{cases} 0 & \text{if } \delta_t > \delta_t^0 \\ K \cdot \left(\delta_t - \delta_t^0\right) & \text{if } \delta_t \le \delta_t^0 \end{cases} \tag{7.1}$$

$$\tau_{lt} = 0 \tag{7.2}$$

$$\tau_{zt} = \begin{cases} 0 & \text{if } |\delta_z| > \left|\delta_z^0\right| \\ K \cdot \left(\delta_z - \delta_z^0\right) & \text{if } |\delta_z| \le \left|\delta_z^0\right| \end{cases} \tag{7.3}$$

with δ_t^0 and δ_z^0 obtained in equations (4.1) and (4.2). The finding from all experiment tests in Figure 6(c) shows the final crack width is about 20%–40% of the maximum crack opening. Therefore, an average value of 30% is taken as average crack closure coefficient, that is, $\mu_t = \mu_z = 0.3$.

The validation of model of three-point bending is done for all four test cases and gives similar agreement; but only the case I2-B is presented here because its configuration is similar to the one of impact layup. Since the failure stresses are set to break as same as in experiment, good onset of load drop is automatically found, as presented in force-displacement curves in Figure 12(a), even if its magnitude is overestimated. This overestimation is due to delamination, that is, the end of lower interface delamination in experiment stops at about the lower support's contact (Figure 13(b)), whilst the simulated delamination goes further, as represented by the damage variable in Figure 13(a). The ratio of the energy release rate to the critical energy release rate between two modes (G_I/G_{Ic} and G_{II}/G_{IIc}) is considered, we found that this overestimation is predominated due to shear mode (mode II), which is supposed due to:

- In practice, at the contact between the supports and specimen there is relatively high compressive pressure affecting inside laminate, therefore G_{IIc} should be increased to reduce the delamination effect in mode II[19]; but this influence is not taken into account in the present model.
- The friction effect at the interface for delamination[7] has not been included in model.

The displacement is continued after the onset of crack formation and the maximum crack opening ($\delta_t^{\max}$ and $\delta_z^{\max}$) is correctly predicted (Figure 12(b)). During unloading, the numerical results also exhibit a good accordance in returning of crack width to 30%

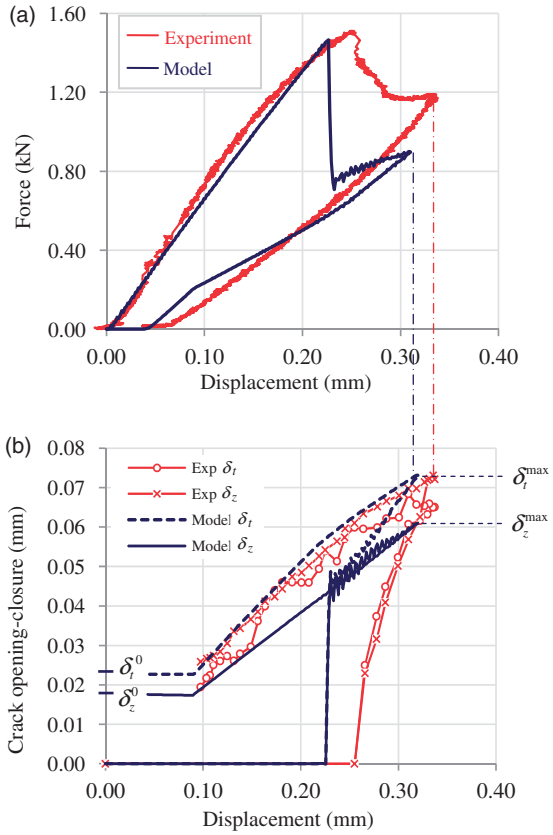

Figure 12. Experimental validation of (a) force-displacement response and (b) crack opening/closure for case study I2-B.

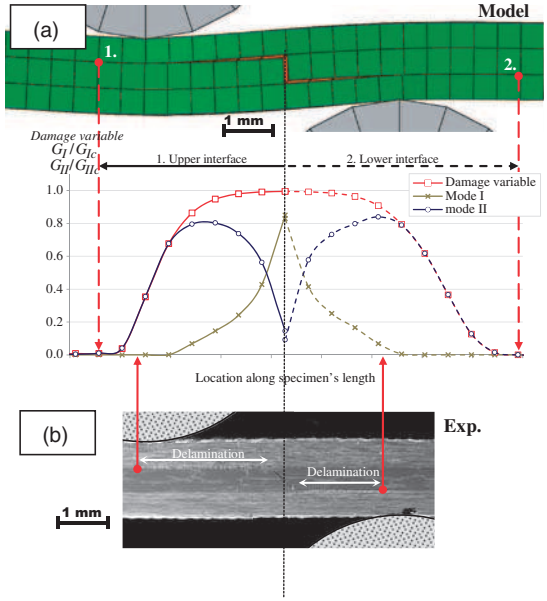

Figure 13. Delamination model of specimen I2-B (a) illustration at maximum crack opening with damage variable and variation of failure mode with respect to location along specimen's length and (b) delamination's length from experiment observed by scanning electron microscope (SEM) compared to model.

of maximum, that is, the final crack-closure width (δ_t^0 and δ_z^0) when the load is totally released.

The three-point bending model presented is a rather qualitative study in order to understand the mechanism of crack opening/closure. The key idea of the proposed law is related to the residual opening of crack as explained above. To simulate the permanent indentation in actual practice, the validation on low-velocity impact model of laminated plate is necessary. Similar to the three-point bending model, the residual opening of each element and each layer is gathered, so the permanent indentation of laminated plate can be formed. However, some differences of their characteristics must be concerned, for example, matrix cracks for three-point bending are free edge, whilst for impact it is internal (closed boundary condition). Therefore, verification of crack closure coefficient on low-velocity impact model is needed.

Verification of permanent indentation law on low-velocity impact modelling

To complete the goal of the study, it is essential to validate the indentation law and crack closure coefficient on low-velocity impact model. The new indentation law is introduced in the existing core of impact model in Ref [3,4]. The permanent indentation concept incorporates with matrix cracking interface in the discrete impact model is still remained. That is, the accumulation of opening of matrix cracks in each ply can contribute to the formation of permanent indentation. Fibre failure also indirectly affects the permanent indentation to be more significant since the fibre failure plies near impact point locally lose their rigidity and induce a great opened block of matrix crack.

Experimental study of low-velocity impact was carried out. T700/M21 laminated (same material as three-point bending specimens) of $150 \times 100 \times 4$ mm^3 plates were fabricated and tested on eight case studies with six different stacking sequences and three impact energies, as detailed in Figure 14. The layups are eight-double-ply, mirror-symmetric, quasi-isotropic, which are made, for this study, in order to facilitate impact damage observation and reduce calculation time. Then, the optimized layup will be the subject of further study after this work is accomplished.

In experiment, permanent indentation of impacted plates is determined by measuring the difference between the lowest point in the dent and the plate surface.[2] Due to twisted form and non-uniform plate surface (Figure 15(b) to (c)), it is necessary to give a definition of surface plate, especially when a precision of permanent indentation is needed. In this study, a fixed distance at about 1.5 of indentor radius, which

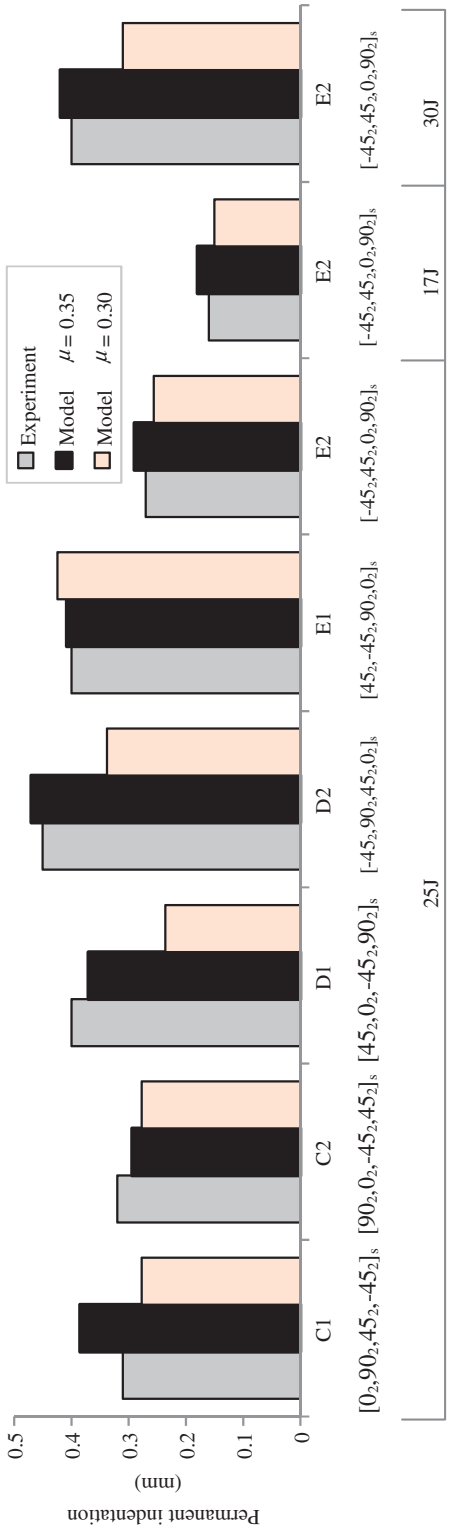

Figure 14. Comparison of permanent indentation on eight test cases, varying layups and impact energies.

is approximately around the dent, is selected to be a representation of average plate surface. Then, permanent indentation can be measured by image correlation technique in 3D.

In order to validate the permanent indentation law, a parametric study of the crack closure coefficient (μ), the single required parameter, was carried out. Figure 14 gives the indentation results of eight test cases which is a comparison between the experiments and the simulations. The influence of tuning the crack closure coefficient is shown, that is, this parameter directly affects the permanent indentation. The parameters $\mu_t = \mu_z = 0.35$ instead of 0.30 from previous section were found to obtain good agreement between experiments and simulations on variation of stacking sequence and impact energy. The different error of the worst case is 24%, which seems acceptable since experimental indentation may be uncertain due to e.g. the scattering of experimental data,[12] relaxation of permanent indentation after 48 hours[8] or the method of measurement as mentioned above. However, the tendency of permanent indentation is well captured.

The result of example case E2 $[-45_2, 45_2, 0_2, 90_2]_s$ at 25 J is showed in Figure 15, demonstrating that the proposed law is able to predict:

- Value and shape of permanent indentation on impacted side (Figure 15(a)–(c)).
- Ply-splitting on non-impacted side due to matrix cracking is simulated, as shown in Figure 15(d)–(e) and No.10–No.10′ in Figure 16, in spite of an overestimation of the simulation (red zone in Figure 15(e)).
- This law also allows the shape of the deformed plate after impact to be obtained as shown by the twisted shape (Figure 15(b)–(e)). The law also allows the creation of residual opening of delamination, according to the interaction with other failure modes, as can be seen from the micrograph in Figure 16(a)–(b). The same sub-numbers indicate the similarity between experiment and simulation at the particular locations.

Although the overestimation of opened delamination in the middle of the layup has been found (Figure 16(b)), it does have small effect on the permanent indentation on impacted side since the permanent indentation is due to the gathering of residual openings of three or four plies on the impacted side as shown in Figure 16(b).

One can notice that the middle of the layup E2 is $[0_2, 90_4, 0_2]$, which is similar to the layup of specimens from three-point bending test I1 $[0, 90_6, 0]$ or I2 $[0_2, 90_2, 0_2]$. The 45° matrix cracking at locations 2, 3 coupling with delamination at locations 6, 7 in Figure 16(a) from

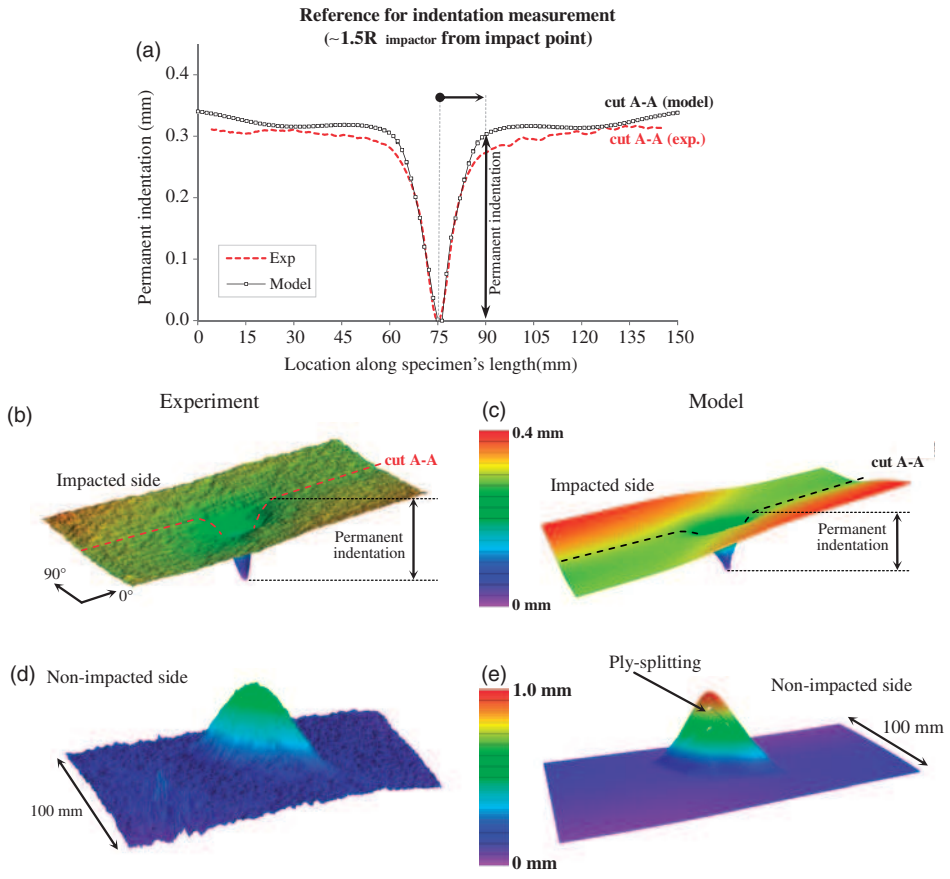

Figure 15. Comparison of permanent indentation for impact test case E2 $[-45_2, 45_2, 0_2, 90_2]_s$ at 25 J.

impact test seems comparable to micrographs from three-point bending tests in Figure 7(a) or Figure 8(a). This can confirm that the choice of using three-point bending test to characterize permanent indentation is reasonable.

Assigning the non-closure crack law into only matrix cracking interfaces is able to contribute not only to the permanent indentation but also the residual opening of delamination. On the contrary, as the present model allows the coupling between matrix cracking and delamination, giving the non-closure crack law at delamination interfaces also seems realistic.

The local plasticity under the indentor is also important for the permanent indentation especially for thick laminates. This topic is currently in progress and will shortly be combined to the global impact model. Thus, the crack closure coefficient may be later adjusted. This point must be studied further.

Conclusion

In the presented paper, a model of permanent indentation due to low-velocity impact was proposed using three-point bending test. An experimental observation of matrix crack opening/closure leads to the idea of permanent indentation formation. When a matrix crack appears, it usually does not completely close and does remain at approximately 30% of maximum crack opening, observed in both transversal and out-of-plane directions. This unclosed crack is due to the blocking of debris inside matrix cracking and cusp formation due to mixed mode (peel and shear) delamination. By taking into account both findings, a simple material law of indentation was proposed according to the unclosed crack which is defined by the crack closure coefficient.

The pseudo-plasticity law was initially tested with three-point bending model based upon a selected case study (I2-B) with the aim of understanding how the crack opening/closure mechanism interacts to the discrete model. Consequently, the same law was validated on low-velocity impact model, and the crack closure coefficient was found to directly affect the value of permanent indentation.

Advantages of the proposed law are its simplicity, and need of only a single parameter which can be found from numerically adjusting the parameter. Also, this law can predict deformed shape of impacted plate

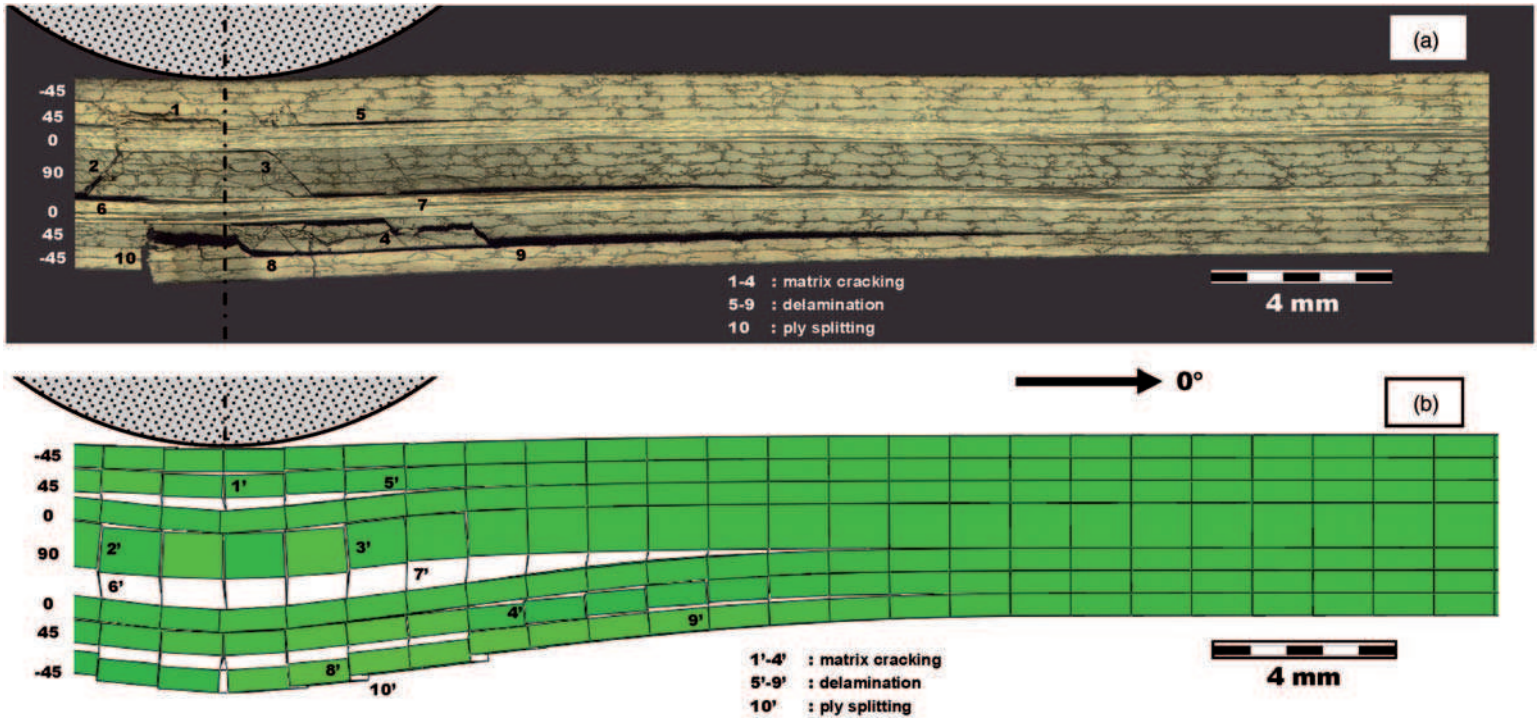

Figure 16. Comparison of longitudinal section cut crossing impact point after impact for impact test case E2 $[-45_2, 45_2, 0_2, 90_2]_s$ at 25 J (a) micrograph from experiment; (b) simulation.

such as twisted form, or opened block of delamination. This benefit is essential for CAI simulation in next step when buckling failure is partially due to plate deflection. On the other hand, it still has some limitations, for example, at high-impact energy with large permanent indentation or penetration, the indentation is mainly governed by the fibre failure, and thus supplementary criterion must be added. However, if the objective is to numerically optimize composite structure at BVID, approximately 0.3 mm–0.6 mm of dent depth,[1] the proposed hypothesis is justified.

Acknowledgements

This work was granted access to the HPC resources of CALMIP under the allocation 2012-P1026.

Funding

The authors gratefully acknowledge the partial financial support through the THEOS Operation Training Program (TOTP).

Conflict of Interest

None declared.

References

1. Rouchon J. Fatigue and damage tolerance aspects for composite aircraft structures. *Delft*1995.
2. ASTM D7136/D7136M. *Standard test method for measuring the damage resistance of a fiber-reinforced polymer matrix composite to a drop-weight impact event*, 2007.
3. Bouvet C, Rivallant S and Barrau J-J. Low velocity impact modeling in composite laminates capturing permanent indentation. *Compos Sci Technol* 2012; 72: 1977–1988.
4. Bouvet C, Hongkarnjanakul N, Rivallant S, et al. Discrete impact modeling of inter- and intra-laminar failure in composites. In: Abrate S, Castanié B and Rajapakse YDS (eds) *Dynamic failure of composite and sandwich structures*. Netherlands: Springer, 2013, pp.339–392.
5. Donadon MV, Iannucci L, Falzon BG, et al. A progressive failure model for composite laminates subjected to low velocity impact damage. *Compos Struct* 2008; 86: 1232–1252.
6. Faggiani A and Falzon BG. Predicting low-velocity impact damage on a stiffened composite panel. *Compos Part A: Appl Sci Manuf* 2010; 41: 737–749.
7. Shi Y, Swait T and Soutis C. Modelling damage evolution in composite laminates subjected to low velocity impact. *Compos Struct* 2012; 94: 2902–2913.
8. Abi Abdallah E, Bouvet C, Rivallant S, et al. Experimental analysis of damage creation and permanent indentation on highly oriented plates. *Compos Sci Technol* 2009; 69: 1238–1245.
9. Caprino G and Lopresto V. The significance of indentation in the inspection of carbon fibre-reinforced plastic panels damaged by low-velocity impact. *Compos Sci Technol* 2000; 60: 1003–1012.
10. Caprino G, Langella A and Lopresto V. Indentation and penetration of carbon fibre reinforced plastic laminates. *Compos Part B: Eng* 2003; 34: 319–325.
11. Chen P, Shen Z, Xiong J, et al. Failure mechanisms of laminated composites subjected to static indentation. *Compos Struct* 2006; 75: 489–495.
12. He W, Guan Z, Li X, et al. Prediction of permanent indentation due to impact on laminated composites based on an elasto-plastic model incorporating fiber failure. *Compos Struct* 2013; 96: 232–242.
13. Laffan MJ, Pinho ST, Robinson P, et al. Measurement of the fracture toughness associated with the longitudinal fibre compressive failure mode of laminated composites. *Compos Part A: Appl Sci Manuf* 2012; 43: 1930–1938.
14. Carbajal N and Mujika F. Determination of compressive strength of unidirectional composites by three-point bending tests. *Polym Test* 2009; 28: 150–156.
15. Mujika F. On the effect of shear and local deformation in three-point bending tests. *Polym Test* 2007; 26: 869–877.
16. Brain WS. Fractography for continuous fiber composites. In: *Engineered materials handbook Vol.1: Composites*. ASM International, 1987.
17. Prombut P. *Caractérisation de la propagation de délaminage des stratifiés composites multidirectionnels*. PhD Thesis, Université de Toulouse, Toulouse, 2007.
18. Cho YB and Averill RC. An improved theory and finite-element model for laminated composite and sandwich beams using first-order zig-zag sublaminate approximations. *Compos Struct* 1997; 37: 281–298.
19. Li X, Hallett SR and Wisnom MR. Predicting the effect of through-thickness compressive stress on delamination using interface elements. *Compos Part A: Appl Sci Manuf* 2008; 39: 218–230.